

# Random matrix analysis of deep neural network weight matrices

Matthias Thamm,\* Max Staats,\* and Bernd Rosenow

*Institut für Theoretische Physik, Universität Leipzig, Brüderstrasse 16, 04103 Leipzig, Germany*

(Dated: March 29, 2022)

Neural networks have been used successfully in a variety of fields, which has led to a great deal of interest in developing a theoretical understanding of how they store the information needed to perform a particular task. We study the weight matrices of trained deep neural networks using methods from random matrix theory (RMT) and show that the statistics of most of the singular values follow universal RMT predictions. This suggests that they are random and do not contain system specific information, which we investigate further by comparing the statistics of eigenvector entries to the universal Porter-Thomas distribution. We find that for most eigenvectors the hypothesis of randomness cannot be rejected, and that only eigenvectors belonging to the largest singular values deviate from the RMT prediction, indicating that they may encode learned information. We analyze the spectral distribution of such large singular values using the Hill estimator and find that the distribution cannot be characterized by a tail index, i.e. is not of power law type.

## I. INTRODUCTION

The application of deep neural networks (DNNs) to a wide range of problems has been tremendously successful in recent years [1–6]. Beyond the classification of images [3], DNNs have been able to learn games beyond human capabilities [7], and have made significant progress in solving hard problems like protein folding [8]. Given these achievements, it is not surprising that neural networks are being applied to a variety of physics problems as well [5]. Applications range from quantum state tomography [9, 10], locating classical [11] and quantum phase transitions [12–15], fluid turbulence [16, 17], troposphere temperature prediction [18] to classifying events in the Large Hadron Collider in search of physics beyond the standard model [19, 20].

Interestingly, successful neural networks are often highly over-parametrized [21–32], such that one might have doubts regarding their capability to generalize beyond the training data set. Furthermore, DNNs can effortlessly memorize large amounts of random training data [33, 34], but still generalize well if there is a rule to be learned. According to the traditional concept of a “bias-variance tradeoff” [35], one would indeed expect these networks to overfit and fail in predicting unseen data. However, it turns out that their generalization capability exhibits a so-called double decent behavior [36–38] as a function of the number of network parameters, such that they perform well in the highly overparametrized limit. The apparent contradiction between overparametrization and good generalization performance is further resolved by emerging evidence that ultra-wide neural networks are inherently biased towards simple functions [6, 39–41]. For the analysis of such highly overparameterised networks we use random matrix theory (RMT) [42–46] as a zero information hypothesis, where deviations from RMT are indications of system

specific information. This approach has already proven to be useful for many other problems with inherent randomness such as the analysis of nuclei spectra [43, 45–47], the investigation of stock market correlations [48–54], and for the analysis of biological networks [55, 56].

Previously RMT has been applied to neural networks for estimating the asymptotic performance of single layer networks [57, 58], and for analyzing the generalization dynamics of linear networks [59]. Other work focused on the spectra of Jacobians at initialization [60] and on the eigenvalue distribution of the Hessian of the loss matrix [61, 62]. The spectral evolution of weight matrices during training was analyzed in [63], with the main results that for smaller or older networks there is a scale in the singular value spectrum separating signal from noise, while in state of the art DNNs the spectral density exhibits a power law tail, reminiscent of the spectrum of heavy-tailed random matrices [64, 65]. These results were subsequently used to assess the quality of pretrained DNNs [66] by computing spectral norms of weight matrices and by assessing the exponent of a power law fit to the tail of the singular value spectrum.

Here, we employ a variety of RMT tools to demonstrate that the weight matrices of modern neural networks are predominantly random. Specifically, we compare the singular values of several DNNs with the Wigner nearest neighbor spacing statistics and find that the bulk of the singular values follows the RMT prediction, even when the networks are fully trained. This finding is also corroborated by the analysis of the number variance of weight matrix singular value spectra. The idea that many singular values do not encode information is tested by comparing the distribution of eigenvector components to the universal Porter-Thomas distribution. Only for a small fraction of eigenvectors with large singular values do we find significant deviations from the Porter-Thomas distribution, indicating that learned information is encoded in them. In addition, we apply the Hill estimator to study the question of whether large singular values of weight matrices can be described by a power law tail of the distribution [63, 66, 67]. In contrast to previous re-

---

\* These authors contributed equally to this work.

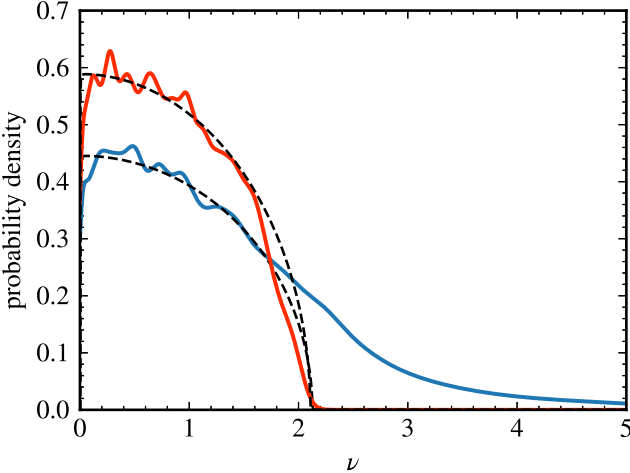


Figure 1. Distribution of the singular values  $\nu$  of the weight matrix of the second hidden layer of a three hidden layer network. The spectral distributions are calculated by broadening with a window size of 15 singular values. The red curve shows the distribution directly after random Glorot initialization, and the blue line depicts the result after fully training the network. The dashed, black lines are fits to the Marchenko-Pastur distribution Eq. (4). After random initialization, the spectrum agrees well with the RMT prediction, and even after training the bulk of the singular values still follows a Marchenko-Pastur distribution with similar parameters.

sults based on fitting the probability density function to a power law, the Hill estimator analysis reveals that the singular value distribution cannot be characterized by a tail exponent, implying that the tail is not described by a power law.

## II. MAIN RESULTS

In this section, we illustrate our main results using the example of a feedforward DNN with three hidden layers, each containing 512 neurons. In the subsequent sections, we provide more details and show that our results are valid more generally for a variety of network architectures. We train the three hidden layer network on the CIFAR-10 dataset [30], which consists of images  $\mathbf{x}^{(k)}$  (3072 pixels each) and corresponding labels  $\mathbf{y}^{(k)}$ , which categorize the images into 10 different classes. Therefore, in total the network has five layers with sizes  $\mathbf{n} = [3072, 512, 512, 512, 10]$ .

Except for the input layer, each layer  $i$  has an associated weight matrix  $\mathbf{W}_i$ , a bias vector  $\mathbf{b}_i$ , and an activation function  $f_i(\mathbf{x})$  which we choose to be a rectified linear unit (ReLU)  $f(x) = \max(x, 0)$  for the hidden layers and softmax  $f_{\text{out}}(\mathbf{x}) = \exp \mathbf{x} / \sum_i \exp x_i$  for the output layer. The activation of the input layer  $\mathbf{a}_0$  is defined as the input image presented to the network

$$\mathbf{a}_0^{(k)} = \mathbf{x}^{(k)}, \quad (1)$$

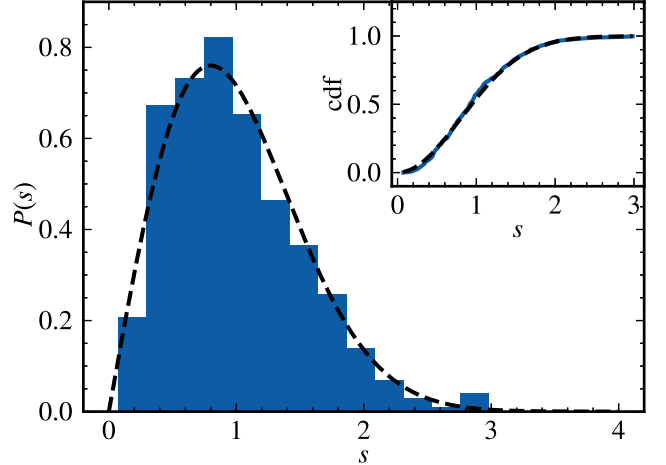


Figure 2. Spacing distributions of unfolded singular values of the weight matrix of the second hidden layer of a trained three hidden layer network. The main panel depicts the probability density histogram and the insets show the cumulative distribution. In addition, the RMT prediction (Wigner surmise) Eq. (5) for matrices from the GOE is indicated by a dashed black line. The prediction is confirmed both visually and by a Kolmogorov-Smirnov test, which at the 40% confidence level cannot reject the hypothesis that the Wigner surmise is the correct distribution.

and then the network propagates the activations through each layer such that the activation in layer  $i$  is given by

$$\mathbf{a}_i^{(k)} = f_i(\mathbf{W}_i \mathbf{a}_{i-1}^{(k)} + \mathbf{b}_i). \quad (2)$$

Here, the  $\mathbf{W}_i$  are  $n_i \times m_i$  weight matrices, with  $n_i$  denoting the width of layer  $i$  and  $m_i$  denoting the width of layer  $i-1$ . The output of the network is defined as the activation of the last layer, using the largest entry of  $\mathbf{a}_{\text{out}}^{(k)}$  as prediction for the class of the input image  $\mathbf{x}^{(k)}$ .

Before training, weights are initialized using the distribution Glorot uniform [68] while the biases are set to zero. Hence the initial weight matrices are random matrices and obey RMT predictions. The network's weights and biases are trained by minimizing the cross-entropy cost function

$$l(\mathbf{W}, \mathbf{b}) = -\frac{1}{N} \sum_{k=1}^N \mathbf{a}_{\text{out}}^{(k)} \cdot \ln(\mathbf{y}^{(k)}) \quad (3)$$

on the training dataset using gradient descent on mini-batches of size 32. Further details of the training procedure are described in Appendix A.

By analyzing the singular values of weight matrices in trained DNNs using methods of RMT, in the following we argue that a large fraction of the weights remains random even after training, while the learned information is encoded in relatively few large singular values and corresponding vectors. We focus on the second fully connected layer of the three hidden layer example network, and obtain the singular values  $\nu$  via the singular value

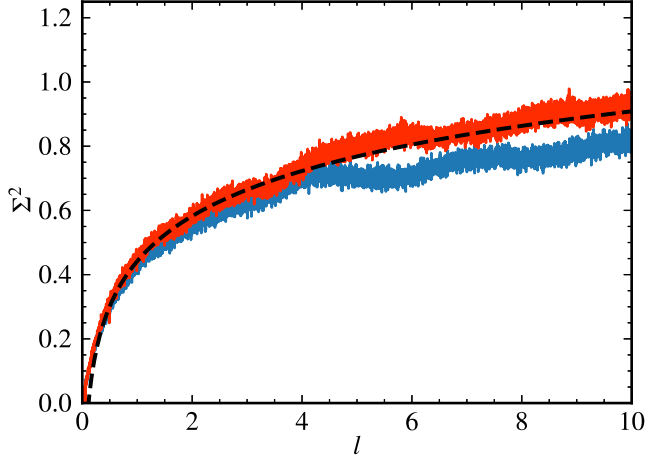


Figure 3. Level number variance  $\Sigma^2$  of singular values of the weights for the second hidden layer of a three hidden layer network, after initialization (red) and after fully training the network (blue). The dashed black line is the theory prediction for the GOE. We find that even after training, the level number variance grows only logarithmically, as predicted by RMT.

decomposition  $W = U \text{diag}(\nu) V^T$  of the corresponding weight matrix  $W$ . Here,  $U$  and  $V$  are orthogonal matrices, and  $\text{diag}(\nu)$  is a diagonal matrix containing the singular values which we assume to be rank-ordered in the following.

We compare the empirical weight matrices to a random control obtained by drawing the entries of an  $n \times m$  matrix independently and identically from a Gaussian probability distribution with variance  $\sigma^2$ , similar to the initialization of weight matrices in a network. The singular values follow the Marchenko-Pastur distribution [69–71],

$$P(\nu) = \begin{cases} \frac{n/m}{\pi\sigma^2\nu} \sqrt{(\nu_{\max}^2 - \nu^2)(\nu^2 - \nu_{\min}^2)} & \nu \in [\nu_{\min}, \nu_{\max}] \\ 0 & \text{else} \end{cases} \quad (4)$$

where  $\nu_{\min} = \tilde{\sigma}(1 \pm \sqrt{m/n})$  and  $\tilde{\sigma} = \sigma\sqrt{n}$ . We assume without loss of generality that  $m \leq n$ . In the case of the second hidden layer weight, we have  $n = m = 512$ . While the distribution Eq. (4) is a parameter free description of the random control (or an untrained network), the trained network deviates from the random control (see also the discussion in [63]). In the absence of a microscopic theory for the spectrum of a trained weight matrix, we estimate its random part by fitting the empirical spectra in the following way: we set  $\nu_{\min}$  equal to the smallest empirical eigenvalue, and then use  $\nu_{\max}$  and  $\sigma^2$  as fit parameters.

Comparing the singular value spectra of the random weights at initialization (red line in Fig. 1) with those of the trained network (blue line in Fig. 1), it becomes apparent that the bulk of the singular values still follows

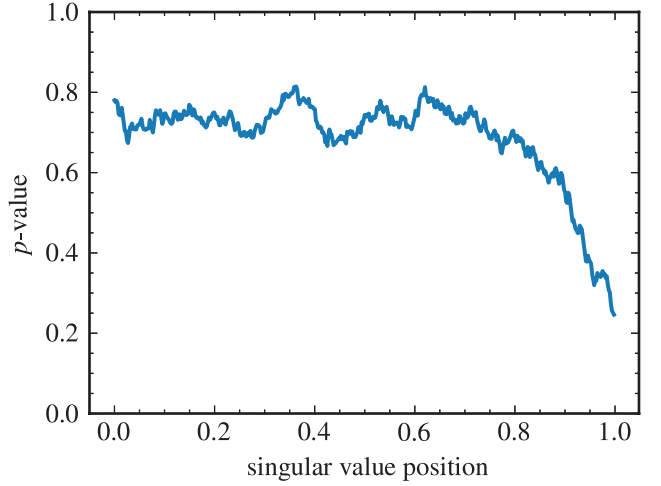


Figure 4. Randomness of eigenvectors as a function of the singular value position in the spectrum: we quantify the agreement with the RMT Porter-Thomas distribution by computing the  $p$ -value of a Kolmogorov-Smirnov test on the entries of the eigenvectors of  $W^*W$  for the second hidden layer of a three hidden layer network. On the  $x$  axis, we plot the positions according to the rank ordered singular values, such that 0 corresponds to the smallest and 1 to the largest singular value of each weight matrix. The results are averaged over neighboring singular values with a window size of 15. For large singular values, the hypothesis of random eigenvectors is rejected, indicating that information is stored in these singular values and eigenvectors.

a Marchenko-Pastur distribution with similar parameters (dashed, black line in Fig. 1). In addition, there are some larger singular values, which do not occur in the spectrum of the random control.

To further see that the majority of singular values of trained networks are indeed random and do not encode information, we consider the distribution of nearest-neighbor spacings of unfolded singular values. Here, unfolding refers to normalizing the mean density of states of the singular values  $\nu_i$  to unity, yielding the unfolded spectrum  $\xi_i$  [42–46]. In contrast to the singular value distribution, which is non-universal and depends on the system at hand, the spacing distribution is a universal property of random matrices. For real random matrices in the universality class of the Gaussian orthogonal ensemble (GOE), the level spacings  $s_k = \xi_{k+1} - \xi_k$ , i.e. the differences between neighboring singular values, are distributed according to the Wigner surmise [42–47]

$$P_{\text{GOE}}(s) = \frac{\pi s}{2} \exp\left(-\frac{\pi}{4}s^2\right). \quad (5)$$

The nearest neighbor spacings of the weight matrix singular values are in excellent agreement with the RMT prediction Eq. (5) even after training the networks (Fig. 2). This is supported by a Kolmogorov-Smirnov test of the empirical data against Eq. (5) that cannot reject the null hypothesis even at a significance level as high as  $\alpha = 0.40$ .

Another prediction of RMT that allows to test the random nature of weight matrices is the level number variance, which shows long range correlations in the spectrum. The number variance describes fluctuations in the number of unfolded singular values  $N_{\xi_i}(l)$  in intervals of length  $l$  around each singular value  $\xi_i$

$$\Sigma^2(l) = \langle (N_{\xi_i}(l) - l)^2 \rangle_{\xi_i}. \quad (6)$$

For random matrices from the GOE universality class, the level number variance depends on the interval width  $\ell$  according to  $\Sigma^2(l) \propto \ln(2\pi l)$  [43–46] (dashed, black line in Fig. 3) in very good agreement with empirical results for the trained example network (Fig. 3). In particular, there are only small differences between randomly initialized weights (red lines in Fig. 3) and the fully trained weight matrices.

In addition, we consider the normalized eigenvectors of the  $m \times m$  matrix  $W^{\dagger}W$  (the right singular vectors of  $W$ ), whose components in the case of a random matrix are described by the Porter-Thomas distribution [43, 45, 46], i.e. a Gaussian distribution with zero mean and standard deviation  $1/\sqrt{m}$ . To verify whether the observation that most singular values of trained networks are random also carries over to the associated eigenvectors, we test the empirical distribution of the entries of each eigenvector against such a Gaussian distribution using a Kolmogorov-Smirnov test. If the test returns a large  $p$ -value, the eigenvector entries are most likely normally distributed and hence contain only noise, while a small  $p$ -value indicates that the Gaussian hypothesis is rejected, which we interpret as evidence for stored information. To reveal a trend in the data, we average the resulting  $p$ -values over neighboring singular values with a window size of 15. Indeed we find that most eigenvectors are random, especially those belonging to small singular values (Fig. 4). For large singular values, we observe a decrease of the  $p$ -values, indicating that relevant information is stored in the corresponding eigenvectors, which is also consistent with the results [63].

We further analyze the tail region of the singular value distribution, which was recently described in terms of power law fits to the probability distribution function [63, 66]. To this end, we consider the eigenvalues  $\lambda = \nu^2$  of the matrix  $W^{\dagger}W$ , and analyze a potential power law decay of the cumulative distribution function using the Hill estimator [72] obtained by averaging the inverse local slopes of the log-log cumulative distribution. A power law tail would manifest itself in an extended flat region of a Hill plot, which is absent in Fig. 5. In Sec. VI we extend this analysis to a variety of modern DNNs and do not find evidence for a power law behavior in any of them, in contrast to the characterization of DNNs in terms of power law fits to the distribution function of weight matrix singular values [63, 66].

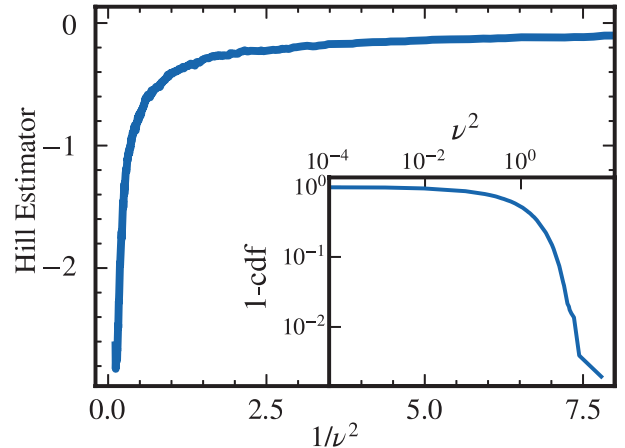


Figure 5. Estimate of the tail exponent of the singular value spectrum of a three hidden layer network obtained by averaging the inverse local slopes obtained via a Hill estimator with windows size  $a = 20$ . The absence of a flat plateau region shows that no power law is present, even though this is not immediately evident in a double logarithmic plot of the cumulative distribution (inset).

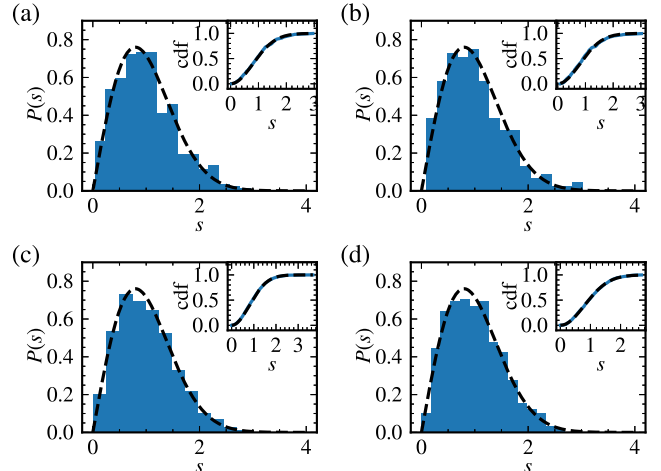


Figure 6. Nearest neighbor spacing distributions of unfolded singular values of weight matrices for various neural networks. The main panels depict the probability density histograms and the insets show the cumulative distribution functions. In addition, we depict the Wigner surmise theory prediction Eq. (5) for the GOE with dashed, black lines. (a) Results for the second hidden layer weight matrix of a three hidden layer network [3072, 1024, 512, 512, 10]. In addition, results for (b) the second convolutional layer in the CNN miniAlexNet, (c) the second fully connected layer in AlexNet, and (d) for the third dense layer in VGG19. In all cases there is excellent visual agreement with the RMT predictions. This is further supported by Kolmogorov-Smirnov tests which cannot reject the null hypothesis at a significance level of (a) 81%, (b) 85%, (c) 31%, and (d) 96%.

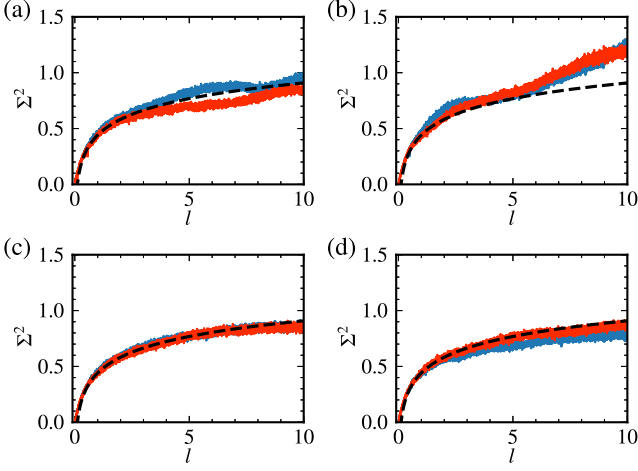


Figure 7. Level number variance of singular values of the weights for (a) the second hidden layer of a three hidden layer network [3072, 1024, 512, 512, 10], (b) the second convolutional layer in the CNN miniAlexNet, (c) the second fully connected layer in AlexNet, and (d) for the third dense layer in VGG19. Red curves show the results for initialized weights and blue lines depict level number variances for fully trained networks. The dashed, black lines depict the theory prediction Eq. (11) for the GOE. In all cases, the level number variance grows logarithmically even after training. Particularly for large networks in (c) and (d), where the statistics are most reliable, deviations from the RMT prediction are small.

### III. UNIVERSALITY OF LEVEL SPACING DISTRIBUTION

To demonstrate that the results presented in the previous section are typical of trained DNNs, we consider several networks with different architectures and sizes here and in the following sections: a) a fully connected feed-forward network with layers of size [3072, 1024, 512, 512, 10] and b) a convolutional network called miniAlexNet consisting of two convolutional layers followed by three dense layers, both trained on the CIFAR-10 [30] dataset. In addition, we analyze the two large networks c) AlexNet [73] and d) VGG19 [31], whose models trained on the ImageNet [74] dataset are available via Matlab and tensorflow [75], respectively. More details on the definition of the networks, training parameters, and performance of the fully trained networks can be found in Appendix A.

In order to compare the various RMT predictions with the properties of empirical weight matrices, we compute their singular value decompositions. While this is straightforward for dense layers, in the case of convolutional layers we first reshape the four dimensional weight tensors to a rectangular shape (for details see App. B) and then compute their singular values and vectors. To obtain smooth probability densities for the singular value spectra, we perform a Gaussian broadening [44, 76] by approximating the probability density as a sum of Gaussian functions centered around each of the  $m$  singular

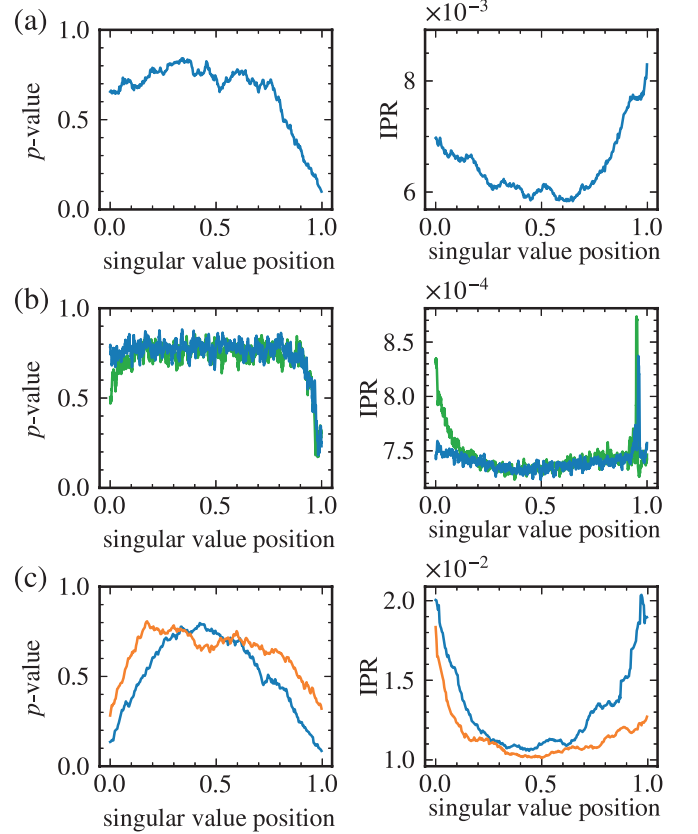


Figure 8. Analysis of the eigenvectors of  $W^\dagger W$ . The left panels depict the  $p$ -values of Kolmogorov-Smirnov tests of the eigenvector entries versus a Gaussian distribution. The right panels show the inverse participation ratios of eigenvectors computed according to Eq. (12). All results are averaged over neighboring eigenvectors with a window size of 15. The  $x$ -direction describes the position of rank ordered singular values, such that 0 corresponds to the smallest and 1 to the largest singular value of each weight matrix. We show results for (a) the second hidden layer of the three hidden layer network [3072, 1024, 512, 512, 10], (b) the first dense layer of the large pretrained DNNs AlexNet (blue) and VGG19 (green), and (c) the second convolutional layer of the CNN miniAlexNet. The results for the  $p$ -values are consistent with those for the inverse participation ratio, indicating that relevant information is stored in eigenvectors corresponding to large singular values.

values  $\nu_k$  with widths  $\sigma_k = (\nu_{k+a} - \nu_{k-a})/2$ , where  $2a$  is the window size of the broadening [51, 77]

$$P(\nu) \approx \frac{1}{m} \sum_{k=1}^m \frac{1}{\sqrt{2\pi\sigma_k^2}} \exp\left(-\frac{(\nu - \nu_k)^2}{2\sigma_k^2}\right). \quad (7)$$

To compare the RMT prediction Eq. (5) with the level spacing of the networks weights, we have to unfold the singular value spectrum first. Here, unfolding is a transformation that maps the singular values  $\nu_i$  to uniformly distributed singular values  $\xi_i$  [42–44, 46, 51]. For this purpose, we first determine the probability density  $P(\nu)$  using Eq. (7) and calculate the corresponding cumulative

Table I. Kolmogorov-Smirnov test results of the distribution of unfolded singular value spacings of the weight matrices against the Brody distribution with  $\beta = 1$ . Rejection of the null hypothesis is based on the  $\alpha = 0.05$  significance level. The p-value indicates how likely it is to obtain a distribution with at least as much cumulative density function deviation as the one tested for drawing random numbers from a Brody distribution with  $\beta = 1$ . In addition, we show the results of a fit of a Brody distribution with free parameter  $\beta$  to the cumulative density function of the computed level spacings. The error was determined by a bootstrap sampling method. We find excellent agreement with the Wigner surmise for a variety of network architectures.

network	reject null hypothesis?			ks-test p-value			Brody $\beta$ from fit		
	layer 1	layer 2	layer 3	layer 1	layer 2	layer 3	layer 1	layer 2	layer 3
three layer [3072,1024,512,512,10] no $L_2$ reg	no	no	no	0.799	0.812	0.792	$0.94 \pm 0.07$	$0.92 \pm 0.11$	$1.03 \pm 0.10$
three layer [3072,1024,512,512,10] with $L_2$	no	no	no	0.196	0.617	0.388	$0.87 \pm 0.07$	$0.90 \pm 0.11$	$1.03 \pm 0.11$
CNN (miniAlexNet) (second conv. layer)	no			0.859			$0.85 \pm 0.14$		
CNN random crop	no			0.354			$0.97 \pm 0.14$		
AlexNet (fc layer)	yes	no	no	0.014	0.344	0.589	$0.90 \pm 0.04$	$0.94 \pm 0.04$	$1.05 \pm 0.08$
VGG16 (fc layer)	no			0.923	0.312	0.309	$0.99 \pm 0.04$	$0.92 \pm 0.04$	$0.92 \pm 0.07$
VGG19 (fc layer)	no			0.376	0.221	0.969	$0.95 \pm 0.04$	$0.92 \pm 0.04$	$0.97 \pm 0.08$

distribution

$$F(\nu) = m \int_{-\infty}^{\nu} P(x) dx. \quad (8)$$

The unfolded singular values are defined as  $\xi_i = F(\nu_i)$ . We then obtain the spacings of the unfolded and sorted singular values  $\xi_i$  via

$$s_k = \xi_{k+1} - \xi_k. \quad (9)$$

We find excellent agreement with the RMT predictions for all network architectures and layers (Fig. 6). This is also supported by Kolmogorov-Smirnov tests (see Tab. I) with null hypothesis that the distribution is described by the Wigner surmise Eq. (5). We infer from the tests that for all network types, for fully connected as well as for convolutional layer, the null hypothesis cannot be rejected on the  $\alpha = 0.05$  significance level (up to a statistically expected number of cases). The  $p$ -values of the Kolmogorov-Smirnov tests (Tab. I) even show that in many cases a rejection for much higher  $\alpha$  is also not possible.

Furthermore, we consider the more general case of a Brody distribution [42, 43, 46]

$$P_{\text{Br}}(s) = B(1 + \beta)s^\beta \exp(-Bs^{1+\beta}), \quad (10)$$

with  $B = \{\Gamma([\beta+2]/[\beta+1])\}^{1+\beta}$ . For  $\beta = 1$  this reduces to the Wigner surmise Eq. (5). Fits of the Brody distribution Eq. (10) to the data show very good agreement with  $\beta \sim 1$  (see Tab. I). To obtain  $\beta$  and the error estimate, we use bootstrap sampling [78–80], fit the Brody distribution to each sample, and then calculate  $\beta$  as the mean and the error as the standard deviation of all fit results.

The level spacing results suggest that the majority of weights is random even after training. This indicates that the weights, even in the case of the large networks trained on ImageNet, have rather low information density.

#### IV. LEVEL NUMBER VARIANCE

The nearest neighbor spacing distribution investigated above probes the level statistics locally. In order to probe long-range correlations between singular values, we compute the level number variance Eq. (6), which is considerably more sensitive to details of the singular value distribution [43, 44]. To determine the level number variance numerically from the unfolded spectrum, for each  $l$  we repeatedly draw values  $\xi_0 \in [\min(\xi_i), \max(\xi_i)]$  and count the number of  $\xi_i$  in the interval  $[\xi_0 - l/2, \xi_0 + l/2]$  and average the variance of this number over the spectrum. For random matrices from the Gaussian Orthogonal Ensemble (GOE) universality class, for large  $l$  the level number variance is given by [43, 44, 46]

$$\Sigma_{\text{GOE}}^2(l) \approx \frac{2}{\pi^2} \left[ \ln(2\pi l) + \gamma + 1 - \frac{\pi^2}{8} \right], \quad (11)$$

where  $\gamma$  is the Euler-Mascheroni constant. It is known for GOE matrices that this formula is also a good approximation in the range of smaller  $l$  [44], but one needs to keep in mind that the level number variance computed for empirical spectra depends on the window size chosen for broadening the spectrum. We find good agreement of Eq. (11) (dashed, black line in Fig. 7) with the results for trained networks (Fig. 7) using a window size  $a = 15$ . In particular, there are only small differences between randomly initialized weights (red lines in Fig. 7) and the fully trained weight matrices.

#### V. DISTRIBUTION OF ENTRIES OF THE SINGULAR VECTORS

In addition to the singular values, we also analyze the singular vectors of the weight matrices of trained DNNs. For an  $n \times m$  weight matrix  $W$ , we consider the eigenvectors of  $W^\dagger W$  (right singular vectors) if  $m \leq n$  or  $WW^\dagger$

(left singular vectors) otherwise. For a completely random matrix of rank  $m$ , RMT predicts that the entries of normalized eigenvectors follow a Gaussian distribution with zero mean and standard deviation  $\sigma = 1/\sqrt{m}$ . We test for agreement between the empirical distribution of the entries of each singular vector with this RMT prediction with the help of the Kolmogorov-Smirnov test, and average the resulting  $p$ -values over neighboring rank ordered singular values with a window size of 15. A large  $p$ -value indicates a random singular vector, as observed for small and intermediate singular values for the three hidden layer network and the large pretrained networks in the left panels of Fig. 8(a) and (b), respectively. For large singular values, the  $p$ -values decrease, suggesting that the Gaussian hypothesis is rejected, and that information is stored in these vectors. For the CNN in Fig. 8(c), we note that eigenvectors corresponding to both small and large singular values show significant deviations from random behavior. However, the resulting matrix  $WW^\dagger$  only has rank 300 which makes the analysis less reliable due to statistical uncertainty.

As a second measure for the randomness of singular vectors, we study their degree of localization as measured by the inverse participation ratio (IPR) [43, 45, 46]

$$\text{IPR}(\mathbf{v}) = \sum_{i=1}^m |v_i|^4. \quad (12)$$

In order to get some intuition for the IPR, we consider two examples: i) for a normalized uniform  $m$ -dimensional vector with equal entries  $1/\sqrt{m}$ , the IPR is given by  $1/m$ , the inverse of the number of relevant components. In the case ii) of a vector with only one non-zero entry, the IPR is equal to unity, again the inverse of the number of relevant components. Since eigenvectors of GOE matrices have many relevant components, the IPR random vectors is on the order of  $1/m$ , while a larger value indicates deviations from RMT and the presence of learned information. This analysis is in very good agreement with that of the  $p$ -values (see right panels in Fig. 8) for large singular values.

## VI. HILL ESTIMATOR FOR TAIL SPECTRA

In previous work [63, 66], it has been argued that the spectral density of the singular values of DNN weight matrices can be fitted by a power law. In order to study the distribution of large singular values further, we employ the Hill estimator for power law tail exponents [72], which has been widely used in the applied finance, economics, and statistics literature [81–87].

For this purpose, we first rank order the eigenvalues  $\lambda_i = \nu_i^2$  of the weight matrices and compute the corresponding cumulative distribution function as

$$F(\lambda_i) = \frac{i}{N} \quad (13)$$

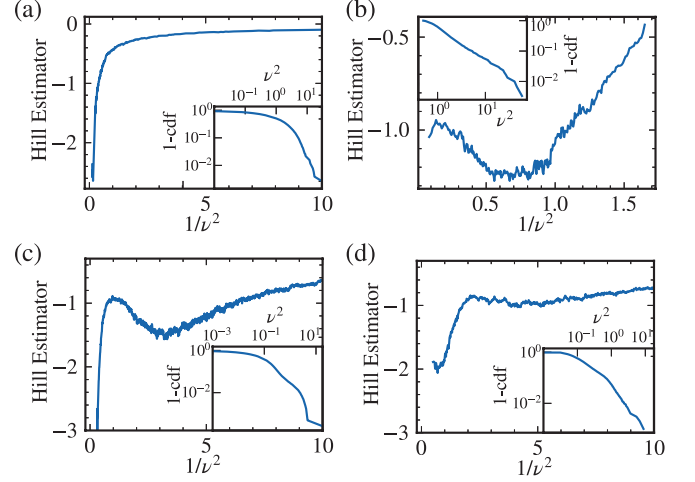


Figure 9. Analysis of the cumulative distribution of DNN singular values in the tail region. Hill estimators of the weight matrix spectra for (a) the second layer weight matrix of a three layer network [3072, 1024, 512, 512, 10], (b) the second convolutional layer of the CNN miniAlexNet, (c) the second fully connected layer of AlexNet, and (d) the third fully connected layer of VGG19. The Hill estimators are obtained using Eq. (15) and Eq. (16) with a window size  $a = 20$ . The insets depict the corresponding log-log cumulative distributions. We do not find evidence of power-law behavior as extensive flat regions are absent.

where a small index corresponds to a small eigenvalue. The Hill estimator  $h$  is then obtained from the local inverse slopes

$$\zeta_i = \frac{-\ln[\lambda_{i+1}/\lambda_i]}{\ln[F(\lambda_{i+1})/F(\lambda_i)]} \quad (14)$$

by averaging over  $2a$  surrounding eigenvalues

$$\tilde{\lambda}_i = \frac{1}{a} \sum_{j=-a}^a \lambda_{i+j} \quad (15)$$

$$h(\tilde{\lambda}_i) = \left( \frac{1}{a} \sum_{j=-a}^a \zeta_{i+j} \right)^{-1}. \quad (16)$$

The Hill estimator is sensitive to changes in the slopes of the log-log cumulative distribution. In the presence of a power law tail, the value of the Hill estimator depends only weakly on the eigenvalue range over which it is determined, and the extrapolation  $1/\lambda^2 \rightarrow 0$  yields the tail exponent of the distribution. According to this criterion, we do not find evidence of power-law tails for either i) a three hidden layer network, ii) miniAlexNet, nor iii) AlexNet (Fig. 9 a-c). Only in the case of VGG19 (Fig. 9d) there is a region of intermediate singular values in the Hill plot with a power law exponent of approximately one, but in the asymptotic regime of large singular values the exponent drops to approximately two, invalidating the concept that a single power law characterizes the distribution. In summary, we find no evidence

that the singular values of DNN weight matrices are described by a power law tail distributions, and argue that the exponent resulting from a power law fit to the singular value probability density function can only be viewed as a heuristic tool to characterize different spectra but not a genuine property of the tail of the distribution of singular values. In addition, given the absence of power law tails in the singular value distribution, it is unclear whether weight matrices of fully trained DNNs indeed belong to an ensemble of heavy tailed random matrices as suggested in [66].

## VII. CONCLUSIONS

The complexity of modern DNNs makes it difficult to understand their learning and generalization behavior. In light of this, we have applied RMT as a zero information hypothesis in order to separate randomness from information. In particular, since at initialization weights are chosen randomly from a probability distribution, the corresponding weight matrices agree perfectly with predictions of RMT before training. Specifically, the singular value spectra of initialized networks are governed by a Marchenko-Pastur distribution, the level spacing distribution follows the Wigner surmise, and the level number variance only grows logarithmically. By comparing these characteristics between randomly initialized and trained networks, one can understand which parts of the weight matrix singular value spectrum stores information.

We find that even in fully trained DNNs large parts of the eigenvalue spectrum remain random. In particular, we demonstrate that the agreement between the level spacing distribution of the bulk of singular values for fully trained networks and the Wigner surmise is statistically highly significant, and that the even more sensitive level number variance continues to agree with the RMT prediction as well. In agreement with the spectra, an analysis of the singular vectors reveals that they are also predominantly random, except for the ones corresponding to the largest singular values. This shows that the majority of the weight matrix does not contain relevant information, and that learned information may be concentrated in the largest singular values and associated vectors only. An analysis of the tails of the eigenvalue spectra using the Hill estimator shows that the distributions are heavy tailed but there is no evidence for a single power law in the tail region of the distribution in any of the cases considered.

## ACKNOWLEDGMENTS

This work has been funded by the Deutsche Forschungsgemeinschaft (DFG) under Grants No. RO 2247/11-1 and No. 406116891 within the Research Training Group RTG 2522/1.

M. T. and M. S. contributed equally to this work.

## APPENDIX A: DETAILS ON NEURAL NETWORKS

In this article, we consider a variety of different networks to show that our results are valid for a wide range of architectures. Tab. II lists the network architectures, training datasets, and accuracies achieved on each dataset. We downloaded the large pre-trained networks vi) AlexNet [73] via Matlab, and vii) VGG16 [31], and viii) VGG19 [31] via tensorflow [75]. Networks i)-v) are trained using mini-batch stochastic gradient descent for 100 epochs. The weights are initialized using the Glorot uniform distribution [68] and the biases are initialized with zeros. We standardize each image of the CIFAR-10 dataset by subtracting the mean and dividing by the standard deviation. We set the learning rate to 0.001 at the beginning and use an exponential learning rate schedule with decay constant 0.95. For all networks, we choose 0.95 as momentum and the mini-batch size is 32. Networks i)-ii) in Tab. II are trained without  $L_2$  regularization, while we use an  $L_2$  regularization strength of  $10^{-4}$  for training networks iii)-v). Network v) uses a technique called random cropping [34], i.e. before passing an image of the CIFAR-10 dataset with size  $32 \times 32$  to the network, it is randomly cropped to size  $28 \times 28$ . Therefore, during each epoch of training, the training dataset is slightly different which can help the network to focus on learning the rule and to reduce overfitting.

## APPENDIX B: RESHAPING OF CONVOLUTIONAL LAYER WEIGHTS

In the case of convolutional layers we have to reshape the filters before computing the singular value decomposition. We unfold the four dimensional weights in such a way that we have as many rows in the matrix as we have three dimensional filters [88]. Each row is filled with the three dimensional filter that is listed with the smallest dimensions last to keep points that are close in the 3D tensor also close in 1D. In formal terms, this means that for a convolutional layer  $W$  of the form  $(K, L, M, N)$ , where without loss of generality  $K > L > M > N$ , the reshaped matrix  $\tilde{W}$  with dimensions  $(K, L \cdot M \cdot N)$  is related to the original matrix in the following way:

$$\tilde{W}_{k,(l \cdot M \cdot N + m \cdot N + n)} = W_{k,l,m,n} \quad (B1)$$

All indices start at zero. While this procedure is to some degree arbitrary we convinced ourselves that similar methods give the same qualitative results.

Table II. Neural network architectures and performance of trained networks. We use d to indicate a dense layer, c for a convolutional layer, p for max pooling, f for flattening, rc for random crop layer, and r for response normalization layer (with a depth radius of 5, a bias of 1,  $\alpha = 1$ , and  $\beta = 0.5$ ).

	network	dataset	training acc	test acc
i)	3 hidden layer {d 3072, d 512, d 512, d 512, d 10} [34]	CIFAR-10	100%	54.7%
ii)	3 hidden layer {d 3072, d 1024, d 512, d 512, d 10} no regularization	CIFAR-10	100%	55.4%
iii)	3 hidden layer {d 3072, d 1024, d 512, d 512, d 10} with $L_2$ regularization	CIFAR-10	100%	56.2%
iv)	miniAlexNet {c 300 5 $\times$ 5, p 3 $\times$ 3, r, c 150 5 $\times$ 5, p 3 $\times$ 3, r, f, d 384, d 192, d 10} [34]	CIFAR-10	100%	78.5%
vi)	AlexNet [73]	ImageNet		57.1%
vii)	VGG16 [31]	ImageNet		67.6%
viii)	VGG19 [31]	ImageNet		71.8%

---

[1] Y. LeCun, Y. Bengio, and G. Hinton, Deep learning, *Nature* **521**, 436 (2015).

[2] I. Goodfellow, Y. Bengio, and A. Courville, *Deep learning* (MIT press, 2016).

[3] A. Krizhevsky, I. Sutskever, and G. E. Hinton, Imagenet classification with deep convolutional neural networks, *Advances in neural information processing systems* **25**, 1097 (2012).

[4] D. Silver, J. Schrittwieser, K. Simonyan, I. Antonoglou, A. Huang, A. Guez, T. Hubert, L. Baker, M. Lai, A. Bolton, *et al.*, Mastering the game of go without human knowledge, *Nature* **550**, 354 (2017).

[5] G. Carleo, I. Cirac, K. Cranmer, L. Daudet, M. Schuld, N. Tishby, L. Vogt-Maranto, and L. Zdeborová, Machine learning and the physical sciences, *Reviews of Modern Physics* **91**, 045002 (2019).

[6] Y. Bahri, J. Kadmon, J. Pennington, S. S. Schoenholz, J. Sohl-Dickstein, and S. Ganguli, Statistical mechanics of deep learning, *Annual Review of Condensed Matter Physics* **11**, 501 (2020).

[7] D. Silver, A. Huang, C. J. Maddison, A. Guez, L. Sifre, G. Van Den Driessche, J. Schrittwieser, I. Antonoglou, V. Panneershelvam, M. Lanctot, *et al.*, Mastering the game of go with deep neural networks and tree search, *Nature* **529**, 484 (2016).

[8] J. Jumper, R. Evans, A. Pritzel, T. Green, M. Figurnov, O. Ronneberger, K. Tunyasuvunakool, R. Bates, A. Žídek, A. Potapenko, *et al.*, Highly accurate protein structure prediction with alphafold, *Nature* **596**, 583 (2021).

[9] G. Torlai, G. Mazzola, J. Carrasquilla, M. Troyer, R. Melko, and G. Carleo, Neural-network quantum state tomography, *Nature Physics* **14**, 447 (2018).

[10] C. Cao, S.-Y. Hou, N. Cao, and B. Zeng, Supervised learning in Hamiltonian reconstruction from local measurements on eigenstates, *Journal of Physics: Condensed Matter* **33**, 064002 (2020).

[11] J. Carrasquilla and R. G. Melko, Machine learning phases of matter, *Nature Physics* **13**, 431 (2017).

[12] E. P. L. van Nieuwenburg, Y.-H. Liu, and S. D. Huber, Learning phase transitions by confusion, *Nature Physics* **13**, 435 (2017).

[13] K. Ch'ng, J. Carrasquilla, R. G. Melko, and E. Khatami, Machine learning phases of strongly correlated fermions, *Physical Review X* **7**, 031038 (2017).

[14] P. Broecker, J. Carrasquilla, R. G. Melko, and S. Trebst, Machine learning quantum phases of matter beyond the fermion sign problem, *Scientific reports* **7**, 1 (2017).

[15] P. Huembeli, A. Dauphin, and P. Wittek, Identifying quantum phase transitions with adversarial neural networks, *Physical Review B* **97**, 134109 (2018).

[16] C. Lee, J. Kim, D. Babcock, and R. Goodman, Application of neural networks to turbulence control for drag reduction, *Physics of Fluids* **9**, 1740 (1997).

[17] X. Jin, S. Cai, H. Li, and G. E. Karniadakis, Nsfnets (navier-stokes flow nets): Physics-informed neural networks for the incompressible navier-stokes equations, *Journal of Computational Physics* **426**, 109951 (2021).

[18] Z. Chen, J. Gao, W. Wang, and Z. Yan, Physics-informed generative neural network: an application to troposphere temperature prediction, *Environmental Research Letters* **16**, 065003 (2021).

[19] J. Duarte, S. Han, P. Harris, S. Jindariani, E. Kreinhar, B. Kreis, J. Ngadiuba, M. Pierini, R. Rivera, N. Tran, *et al.*, Fast inference of deep neural networks in fpgas for particle physics, *Journal of Instrumentation* **13** (07), P07027.

[20] D. Guest, K. Cranmer, and D. Whiteson, Deep learning and its application to lhc physics, *Annual Review of Nuclear and Particle Science* **68**, 161 (2018).

[21] Y. LeCun, L. Bottou, Y. Bengio, and P. Haffner, Gradient-based learning applied to document recognition, *Proceedings of the IEEE* **86**, 2278 (1998).

[22] Y. LeCun, P. Haffner, L. Bottou, and Y. Bengio, Object Recognition with Gradient-Based Learning, in *Shape, Contour and Grouping in Computer Vision* (Springer, Berlin, Heidelberg, 1999) pp. 319–345.

[23] R. Pascanu, Y. N. Dauphin, S. Ganguli, and Y. Bengio, On the saddle point problem for non-convex optimization, preprint arXiv:1405.4604 (2014).

[24] Y. Dauphin, R. Pascanu, C. Gulcehre, K. Cho, S. Ganguli, and Y. Bengio, Identifying and attacking the saddle point problem in high-dimensional non-convex optimization, preprint arXiv:1406.2572 (2014).

[25] I. J. Goodfellow, O. Vinyals, and A. M. Saxe, Qualitatively characterizing neural network optimization problems, preprint arXiv:1412.6544 (2015).

[26] B. Neyshabur, S. Bhojanapalli, D. McAllester, and N. Srebro, Exploring Generalization in Deep Learning, preprint arXiv:1706.08947 (2017).

[27] D. Soudry and E. Hoffer, Exponentially vanishing sub-optimal local minima in multilayer neural networks, preprint arXiv:1702.05777 (2017).

[28] Siyuan Ma, Raef Bassily, and Mikhail Belkin, The Power of Interpolation: Understanding the Effectiveness of SGD in Modern Over-parametrized Learning, International Conference on Machine Learning , 3325 (2018).

[29] K. Kawaguchi, L. P. Kaelbling, and Y. Bengio, Generalization in deep learning, arXiv preprint arXiv:1710.05468 (2017).

[30] A. Krizhevsky, G. Hinton, *et al.*, Learning multiple layers of features from tiny images, *Tech Report* (2009).

[31] K. Simonyan and A. Zisserman, Very Deep Convolutional Networks for Large-Scale Image Recognition, preprint arXiv:1409.1556 (2014).

[32] X. Zhai, A. Kolesnikov, N. Houlsby, and L. Beyer, Scaling Vision Transformers, preprint arXiv:2106.04560 (2021).

[33] J. Lever, M. Krzywinski, and N. Altman, Points of significance: model selection and overfitting, *Nature methods* **13**, 703 (2016).

[34] C. Zhang, S. Bengio, M. Hardt, B. Recht, and O. Vinyals, Understanding deep learning (still) requires rethinking generalization, *Communications of the ACM* **64**, 107 (2021).

[35] S. Geman, E. Bienenstock, and R. Doursat, Neural Networks and the Bias/Variance Dilemma, *Neural Computation* **4**, 1 (1992).

[36] M. Belkin, D. Hsu, S. Ma, and S. Mandal, Reconciling modern machine-learning practice and the classical bias-variance trade-off, *Proceedings of the National Academy of Sciences* **116**, 15849 (2019).

[37] P. Nakkiran, G. Kaplun, Y. Bansal, T. Yang, B. Barak, and I. Sutskever, Deep double descent: Where bigger models and more data hurt, preprint arXiv:1912.02292 (2019).

[38] M. Belkin, D. Hsu, and J. Xu, Two Models of Double Descent for Weak Features, *SIAM Journal on Mathematics of Data Science* **2**, 1167 (2020).

[39] G. De Palma, B. T. Kiani, and S. Lloyd, Random deep neural networks are biased towards simple functions, preprint arXiv:1812.10156 (2018).

[40] G. Valle-Perez, C. Q. Camargo, and A. A. Louis, Deep learning generalizes because the parameter-function map is biased towards simple functions, preprint arXiv:1805.08522 (2018).

[41] O. Cohen, O. Malka, and Z. Ringel, Learning curves for overparametrized deep neural networks: A field theory perspective, *Physical Review Research* **3**, 023034 (2021).

[42] T. A. Brody, J. Flores, J. B. French, P. A. Mello, A. Pandey, and S. S. M. Wong, Random-matrix physics: spectrum and strength fluctuations, *Reviews of Modern Physics* **53**, 385 (1981).

[43] T. Guhr, A. Müller-Groeling, and H. A. Weidenmüller, Random-matrix theories in quantum physics: common concepts, *Physics Reports* **299**, 189 (1998).

[44] M. L. Mehta, *Random matrices*, 3rd ed., Pure and applied mathematics, Vol. v. 142 (Elsevier/Academic Press, Amsterdam and San Diego, CA, 2004).

[45] T. Papenbrock and H. A. Weidenmüller, Colloquium: Random matrices and chaos in nuclear spectra, *Reviews of Modern Physics* **79**, 997 (2007).

[46] H. A. Weidenmüller and G. E. Mitchell, Random matrices and chaos in nuclear physics: Nuclear structure, *Reviews of Modern Physics* **81**, 539 (2009).

[47] E. P. Wigner, On the statistical distribution of the widths and spacings of nuclear resonance levels, in *Mathematical Proceedings of the Cambridge Philosophical Society*, Vol. 47 (Cambridge University Press, 1951) pp. 790–798.

[48] V. Plerou, P. Gopikrishnan, B. Rosenow, L. A. N. Amaral, and H. E. Stanley, Universal and nonuniversal properties of cross correlations in financial time series, *Physical Review Letters* **83**, 1471 (1999).

[49] L. Laloux, P. Cizeau, J.-P. Bouchaud, and M. Potters, Noise Dressing of Financial Correlation Matrices, *Physical Review Letters* **83**, 1467 (1999).

[50] L. Laloux, P. Cizeau, M. Potters, and J.-P. Bouchaud, Random Matrix Theory and Financial Correlations, *International Journal of Theoretical and Applied Finance* **03**, 391 (2000).

[51] V. Plerou, P. Gopikrishnan, B. Rosenow, L. A. N. Amaral, T. Guhr, and H. E. Stanley, Random matrix approach to cross correlations in financial data, *Physical Review E* **65**, 066126 (2002).

[52] B. Rosenow, V. Plerou, P. Gopikrishnan, and H. E. Stanley, Portfolio optimization and the random magnet problem, *Europhysics Letters (EPL)* **59**, 500 (2002).

[53] R. Schäfer, N. F. Nilsson, and T. Guhr, Power mapping with dynamical adjustment for improved portfolio optimization, *Quantitative Finance* **10**, 107 (2010), <https://doi.org/10.1080/14697680902748498>.

[54] J. Bun, J.-P. Bouchaud, and M. Potters, Cleaning large correlation matrices: Tools from random matrix theory, *Physics Reports* **666**, 1 (2017).

[55] F. Luo, Y. Yang, J. Zhong, H. Gao, L. Khan, D. K. Thompson, and J. Zhou, Constructing gene co-expression networks and predicting functions of unknown genes by random matrix theory, *BMC Bioinformatics* **8**, 299 (2007).

[56] Y. Deng, Y.-H. Jiang, Y. Yang, Z. He, F. Luo, and J. Zhou, Molecular ecological network analyses, *BMC Bioinformatics* **13**, 113 (2012).

[57] C. Louart, Z. Liao, and R. Couillet, A random matrix approach to neural networks, *The Annals of Applied Probability* **28**, 1190 (2018).

[58] J. Pennington and P. Worah, Nonlinear random matrix theory for deep learning, *Journal of Statistical Mechanics: Theory and Experiment* **2019**, 124005 (2019).

[59] A. K. Lampinen and S. Ganguli, An analytic theory of generalization dynamics and transfer learning in deep linear networks, preprint arXiv:1809.10374 (2018), arXiv:1809.10374 [stat.ML].

[60] J. Pennington, S. Schoenholz, and S. Ganguli, The emergence of spectral universality in deep networks, in *Proceedings of the Twenty-First International Conference on Artificial Intelligence and Statistics*, Proceedings of Machine Learning Research, Vol. 84, edited by A. Storkey and F. Perez-Cruz (PMLR, 2018) pp. 1924–1932.

[61] N. P. Baskerville, D. Granziol, and J. P. Keating, Applicability of Random Matrix Theory in Deep Learning, preprint arXiv:2102.06740.

[62] D. Granziol, Beyond random matrix theory for deep networks, preprint arXiv:2006.07721 (2020).

[63] C. H. Martin and M. W. Mahoney, Implicit self-regularization in deep neural networks: Evidence from random matrix theory and implications for learning, *Journal of Machine Learning Research* **22**, 1 (2021).

[64] P. Cizeau and J. P. Bouchaud, Theory of lévy matrices, *Phys. Rev. E* **50**, 1810 (1994).

[65] E. Tarquini, G. Biroli, and M. Tarzia, Level statistics and localization transitions of lévy matrices, *Phys. Rev. Lett.* **116**, 010601 (2016).

[66] C. H. Martin, T. S. Peng, and M. W. Mahoney, Predicting trends in the quality of state-of-the-art neural networks without access to training or testing data, *Nature Communications* **12**, 4122 (2021).

[67] C. H. Martin and M. W. Mahoney, Implicit self-regularization in deep neural networks: Evidence from random matrix theory and implications for learning, *Journal of Machine Learning Research* **22**, 1 (2021).

[68] Xavier Glorot and Yoshua Bengio, Understanding the difficulty of training deep feedforward neural networks, *Proceedings of the Thirteenth International Conference on Artificial Intelligence and Statistics* , 249 (2010).

[69] V. A. Marčenko and L. A. Pastur, Distribution of eigenvalues for some sets of random matrices, *Mathematics of the USSR-Sbornik* **1**, 457 (1967).

[70] A. M. Sengupta and P. P. Mitra, Distributions of singular values for some random matrices, *Physical Review E* **60**, 3389 (1999).

[71] L. Denby and C. Mallows, Computing sciences and statistics: Proceedings of the 23rd symposium on the interface, edited by em keramidas, Interface Foundation, Fairfax Station, VA , 54 (1991).

[72] B. M. Hill, A simple general approach to inference about the tail of a distribution, *The annals of statistics* , 1163 (1975).

[73] A. Krizhevsky, I. Sutskever, and G. E. Hinton, ImageNet classification with deep convolutional neural networks, *Communications of the ACM* **60**, 84 (2017).

[74] J. Deng, W. Dong, R. Socher, L.-J. Li, K. Li, and L. Fei-Fei, Imagenet: A large-scale hierarchical image database, in *2009 IEEE conference on computer vision and pattern recognition* (Ieee, 2009) pp. 248–255.

[75] M. Abadi, A. Agarwal, P. Barham, E. Brevdo, Z. Chen, C. Citro, G. S. Corrado, A. Davis, J. Dean, M. Devin, S. Ghemawat, I. Goodfellow, A. Harp, G. Irving, M. Isard, Y. Jia, R. Jozefowicz, L. Kaiser, M. Kudlur, J. Levenberg, D. Mané, R. Monga, S. Moore, D. Murray, C. Olah, M. Schuster, J. Shlens, B. Steiner, I. Sutskever, K. Talwar, P. Tucker, V. Vanhoucke, V. Vasudevan, F. Viégas, O. Vinyals, P. Warden, M. Wattenberg, M. Wicke, Y. Yu, and X. Zheng, TensorFlow: Large-scale machine learning on heterogeneous systems (2015), software available from tensorflow.org.

[76] M. Brack, J. Damgaard, A. S. Jensen, H. C. Pauli, V. M. Strutinsky, and C. Y. Wong, Funny Hills: The Shell-Correction Approach to Nuclear Shell Effects and Its Applications to the Fission Process, *Reviews of Modern Physics* **44**, 320 (1972).

[77] H. Bruus and J.-C. A. d’Auriac, The spectrum of the two-dimensional Hubbard model at low filling, *Europhysics Letters (EPL)* **35**, 321 (1996).

[78] B. Efron, Bootstrap Methods: Another Look at the Jackknife, *The Annals of Statistics* **7** (1979).

[79] B. Efron and R. Tibshirani, *An introduction to the bootstrap*, [nachdr.] ed., Monographs on statistics and applied probability, Vol. 57 (Chapman & Hall, Boca Raton, Fla., 1998).

[80] B. Efron, Second Thoughts on the Bootstrap, *Statistical Science* **18**, 135 (2003).

[81] V. Akgiray and G. G. Booth, The siable-law model of stock returns, *Journal of Business & Economic Statistics* **6**, 51 (1988).

[82] B. Cheng and S. T. Rachev, Multivariate stable futures prices, *Mathematical Finance* **5**, 133 (1995).

[83] P. Gopikrishnan, V. Plerou, L. A. N. Amaral, M. Meyer, and H. E. Stanley, Scaling of the distribution of fluctuations of financial market indices, *Physical Review E* **60**, 5305 (1999).

[84] T. Lux, The stable parettian hypothesis and the frequency of large returns: an examination of major german stocks, *Applied financial economics* **6**, 463 (1996).

[85] C. Quintos, Z. Fan, and P. C. Phillips, Structural change tests in tail behaviour and the asian crisis, *The Review of Economic Studies* **68**, 633 (2001).

[86] N. H. Chan, S.-J. Deng, L. Peng, and Z. Xia, Interval estimation of value-at-risk based on garch models with heavy-tailed innovations, *Journal of Econometrics* **137**, 556 (2007).

[87] J. B. Hill, On tail index estimation for dependent, heterogeneous data, *Econometric Theory* **26**, 1398 (2010).

[88] Y. Yoshida and T. Miyato, Spectral norm regularization for improving the generalizability of deep learning, preprint arXiv:1705.10941 (2017).